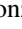










The Chemistry of Cosmic Dust Analogs from C, C₂, and C₂H₂ in C-rich Circumstellar Envelopes

Gonzalo Santoro¹ , Lidia Martínez¹, Koen Lauwaet², Mario Accolla¹ , Guillermo Tajuelo-Castilla¹, Pablo Merino^{1,3}, Jesús M. Sobrado⁴, Ramón J. Peláez⁵, Víctor J. Herrero⁵, Isabel Tanarro⁵, Álvaro Mayoral⁶, Marcelino Agúndez³ , Hassan Sabbah⁷ , Christine Joblin⁷ , José Cernicharo³ , and José Ángel Martín-Gago¹ 

¹ Instituto de Ciencia de Materiales de Madrid (ICMM. CSIC). Materials Science Factory. Structure of Nanoscopic Systems Group. c/Sor Juana Inés de la Cruz 3, E-28049 Cantoblanco, Madrid, Spain; gonzalo.santoro@icmm.csic.es, gago@icmm.csic.es

² IMDEA Nanociencia. Ciudad Universitaria de Cantoblanco, E-28049 Cantoblanco, Madrid, Spain

³ Instituto de Física Fundamental (IFF. CSIC). Group of Molecular Astrophysics. c/Serrano 123, E-28006 Madrid, Spain

⁴ Centro de Astrobiología (CAB. INTA-CSIC). Crta- de Torrejón a Ajalvir km4, E-28850, Torrejón de Ardoz, Madrid, Spain

⁵ Instituto de Estructura de la Materia (IEM.CSIC). Molecular Physics Department. c/Serrano 123, E-28006 Madrid, Spain

⁶ School of Physical Science and Technology, ShanghaiTech University, 393 Middle Huaxia Road, Pudong, Shanghai, 201210, People's Republic of China

⁷ IRAP, Université de Toulouse, CNRS, CNES. 9 Av. du Colonel Roche, F-31028 Toulouse Cedex 4, France

Received 2020 January 31; revised 2020 April 21; accepted 2020 May 4; published 2020 June 2

Abstract

Interstellar carbonaceous dust is mainly formed in the innermost regions of circumstellar envelopes around carbon-rich asymptotic giant branch stars (AGBs). In these highly chemically stratified regions, atomic and diatomic carbon, along with acetylene, are the most abundant species after H₂ and CO. In a previous study, we addressed the chemistry of carbon (C and C₂) with H₂ showing that acetylene and aliphatic species form efficiently in the dust formation region of carbon-rich AGBs whereas aromatics do not. Still, acetylene is known to be a key ingredient in the formation of linear polyacetylenic chains, benzene, and polycyclic aromatic hydrocarbons (PAHs), as shown by previous experiments. However, these experiments have not considered the chemistry of carbon (C and C₂) with C₂H₂. In this work, by employing a sufficient amount of acetylene, we investigate its gas-phase interaction with atomic and diatomic carbon. We show that the chemistry involved produces linear polyacetylenic chains, benzene, and other PAHs, which are observed with high abundances in the early evolutionary phase of planetary nebulae. More importantly, we have found a nonnegligible amount of pure and hydrogenated carbon clusters as well as aromatics with aliphatic substitutions, both being a direct consequence of the addition of atomic carbon. The incorporation of alkyl substituents into aromatics can be rationalized by a mechanism involving hydrogen abstraction followed by methyl addition. All the species detected in the gas phase are incorporated into nanometric-sized dust analogs, which consist of a complex mixture of sp, sp², and sp³ hydrocarbons with amorphous morphology.

Unified Astronomy Thesaurus concepts: Asymptotic giant branch (108); Post-asymptotic giant branch (1287); Circumstellar matter (241); Circumstellar dust (236); Laboratory astrophysics (2004); Molecular physics (2058); Plasma physics (2089); Protoplanetary nebulae (1301)

1. Introduction

Carbonaceous dust is ubiquitously found in space, from the interstellar medium (ISM) to nova ejecta and circumstellar shells (Chiar et al. 2013). Astronomical observations in the mid-infrared (MIR) range reveal the presence of both aromatic and aliphatic dust components. In the diffuse ISM, the 3.4 μm absorption band (assigned to the CH vibrational stretching modes of CH₂ and CH₃ aliphatic moieties), along with the weaker absorption features at 6.8 and 7.3 μm (which correspond to the CH bending modes of aliphatic groups), have been attributed to hydrogenated amorphous carbon (Pendleton & Allamandola 2002; Dartois et al. 2004). On the other hand, the so-called aromatic infrared emission bands (AIBs) are widely observed in environments of our Galaxy that are submitted to ultraviolet (UV) photons (Peeters et al. 2002, 2004). The AIBs, which fall in the spectral range from 3 to 20 μm (main bands at 3.3, 6.2, 7.7, 8.6 and 11.2 μm) have generally been assigned to polyaromatic carriers that are small enough to be stochastically heated by the absorption of a single UV photon, which constitutes the polycyclic aromatic hydrocarbon (PAH) hypothesis (Leger & Puget 1984; Allamandola et al. 1985, 1989; Puget & Leger 1989). There is also

observational evidence for an evolutionary scenario from aliphatics to aromatics calling for very small grains of mixed aliphatic–aromatic composition both in evolved star environments (Goto et al. 2003; Kwok & Zhang 2011) and in molecular clouds (Pillari et al. 2015). Overall, these observations call for a better understanding of the formation of PAHs and of carbon dust in general in astrophysical environments.

In our Galaxy, carbon-rich (C-rich) asymptotic giant branch (AGB) stars are the major sources of carbonaceous dust (Gehrz 1989), thus chemical models have been developed to account for the formation of PAHs and hydrogenated carbon clusters in these environments (e.g., Pascoli & Polleux 2000; Cherchneff 2011). According to observations, acetylene (C₂H₂) is one of the most abundant molecules in the inner regions of circumstellar envelopes (CSEs) where dust is formed, presenting a relative abundance to H₂ of 8 × 10^{−5} (Fonfría et al. 2008), while carbon atoms are also expected to be highly abundant. Chemical equilibrium calculations predict the concentration of carbon atoms to be 1–2 orders of magnitude below that of C₂H₂ in the region where carbon molecules are expected to condense into dust (Agúndez et al. 2020).

It is well known that the polymerization of C_2H_2 gives rise to polyacetylenic chains (Cernicharo 2004), whose formation mechanism has been recently mapped with the Atacama Large Millimeter/submillimeter Array in the outer regions of the C-star envelope IRC +10216 (Agúndez et al. 2017). Furthermore, diacetylene (C_4H_2) has been recently detected in this star through high spectral resolution MIR observations (Fonfría et al. 2018). Acetylene is also believed to play a crucial role in the formation of benzene and PAH compounds (Frenklach & Feigelson 1989). The formation of benzene in evolved stars has been rationalized from experiments of C_2H_2 pyrolysis by the reaction of two propargyl (C_3H_3) radicals (Miller & Melius 1992), a mechanism that requires high temperatures and high acetylene concentrations, which are not encountered in the dust nucleation zone of AGB stars. The temperature in the region between two and four stellar radii is estimated to range from 1500 to 1000 K whereas a density of acetylene of 10^7 – 10^5 molecules cm^{-3} has been derived by Fonfría et al. (2008). This abundance for acetylene is in very good agreement with recent model predictions for C-rich AGB stars (Agúndez et al. 2020).

Another chemical route for the formation of benzene, considering neutral–neutral reactions, and at much lower temperatures than those needed in combustion theory, has been derived from acetylene discharges. It proceeds mainly by the addition of C_2H_2 to the C_4H_3 radical and to a lesser extent by the cyclization of C_6H_4 (De Bleeker et al. 2006a). Further growth from benzene to PAHs is assumed to take place through the so-called hydrogen abstraction acetylene addition (HACA) mechanism (Frenklach & Warnatz 1987; Frenklach & Feigelson 1989; Shukla & Koshi 2012; Yang et al. 2016). Recently, a chemical route for the growth of large benzoid-PAHs (comprised only of six-membered ring structures) has been proposed through the so-called hydrogen abstraction vinylacetylene addition (HAVA) mechanism (Zhao et al. 2018). Thus, complementary HACA/HAVA mechanisms might be needed for the molecular growth of PAHs in circumstellar environments.

Several laboratory experiments have dealt with the formation of stardust analogs from acetylene, either in dusty plasmas (Kovačević et al. 2005; Stefanović et al. 2005), in pyrolysis experiments (Biennier et al. 2009; Jäger et al. 2009) or in molecular jets exposed to plasma discharges (Contreras & Salama 2013). However, all of them lack the addition of atomic carbon and therefore are not suitable for evaluating its impact on the growth of hydrocarbons with implications on, e.g., the formation of hydrocarbons with an odd number of carbon atoms (Cernicharo 2004).

Recently, we have shown that sputtering gas aggregation sources (SGASs) are particularly suited for studying dust formation in the CSE of AGBs (Martínez et al. 2020). In particular, we have demonstrated that the interaction of atomic carbon with molecular hydrogen promotes the formation of nonaromatic molecules, acetylene being one of the main gas-phase products. Here, we expand our previous work to investigate the interaction of atomic carbon with acetylene due to its known importance in the formation and growth of hydrocarbons. In order to accelerate the chemistry between carbon and acetylene so as to have access to most of the reaction pathways, as well as to investigate different conditions which would pertain to different regions of the CSE, we have intentionally increased the concentration of acetylene. In

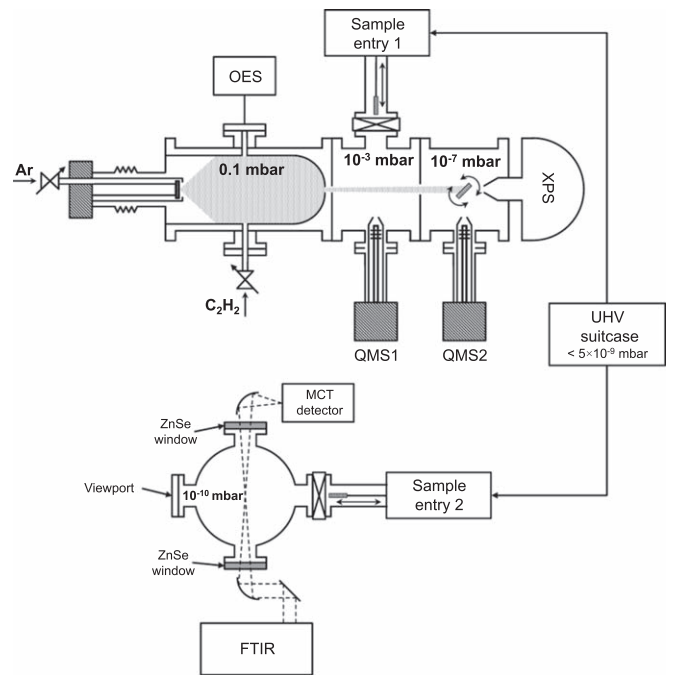


Figure 1. Scheme of the experimental setup used for the analog production and analysis. The pressure at each ultrahigh vacuum chamber during the formation of the analogs is indicated.

addition, our experimental conditions are also of interest for studying the envelopes of C-rich protoplanetary nebulae (PPNe) in which the UV radiation from the central star provokes the photodissociation of acetylene and methane, providing a high abundance of carbon initiating a rich chemistry involving C, C_2H_2 , CH_4 and other hydrocarbons (Cernicharo 2004).

We have found that, unlike what is commonly observed for dust analogs prepared in pyrolysis experiments or plasmas, a nonnegligible amount of the produced material consists of carbon clusters (both pure and hydrogenated) with an odd number of carbon atoms, being a direct consequence of the interaction of atomic carbon with acetylene. Additionally, aromatics with aliphatic substitutions have been observed. We suggest that the formation of alkyl-substituted aromatics proceeds through the formation of CH_3 radicals, which is also a consequence of the addition of atomic carbon.

2. Experiments

For the production and analysis of the dust analogs we employed the Stardust machine. The technical details of Stardust can be found elsewhere (Martínez et al. 2018, 2020). The particular experimental setup used in this work is schematically depicted in Figure 1. A pictorial view of the CSE region simulated by our experimental setup can be found in Martínez et al. (2020). The base pressure of the system is in the 10^{-10} mbar range and the pressure during the production of the analogs at different positions of the machine is also indicated in Figure 1.

Dust analogs were produced with a scaled-up multiple ion cluster source (MICS) (Martínez et al. 2012), a special type of SGAS, working in ultrahigh vacuum (UHV) conditions (Haberland et al. 1991). Atomic carbon was delivered by magnetron sputtering of a 2 inch graphite target (99.95% purity) using Ar as sputtering gas with a flow rate of 150 sccm.

The sputtered atoms coalesce inside the aggregation zone (aggregation length, i.e., distance from the magnetron target to the exit nozzle: 374 mm). Acetylene (purity $\geq 99.6\%$, diluted in acetone) was injected in the aggregation zone of the MICS through a lateral entrance at constant flow rates of 0, 4×10^{-4} , 0.15, and 1 sccm. The DC magnetron was regulated in current and 0.2 A (corresponding to 100 W) were applied.

Optical emission spectroscopy (OES) was performed inside the aggregation zone (at OES position in Figure 1) and the light emitted by the sputtering plasma at a distance of around 1 cm from the magnetron target was collected through a fused silica window and a fused silica optical fiber. A 193 mm focal length, motorized Czerny–Turner spectrograph (Andor, model Shamrock SR-193-i-A) equipped with a CCD camera (iDus DU420A-BVF) was employed. Two diffraction gratings with 1200 and 1800 grooves mm^{-1} , installed in a movable turret, provide spectral ranges of 300–1200 nm and 200–950 nm, respectively, and nominal spectral resolutions of 0.22 nm and 0.15 nm, respectively (for an input slit width of $20 \mu\text{m}$). The relative spectral efficiencies of the spectroscopic equipment were quantified for both diffraction gratings with a calibrated tungsten lamp.

Mass spectrometry was used for in situ analysis of the gaseous species produced during the production of the dust analogs. This was performed at positions labeled as QMS1 and QMS2 in Figure 1. At QMS1 a quadrupole mass spectrometer (PrismaPlus, Pfeiffer) with a mass range of 0–100 amu and a Faraday cup detector was used. At QMS2, a Pfeiffer HiQuad QMG 700 with QMA 400 mass spectrometer (mass range of 0–512 amu) equipped with a CP 400 ion counter preamplifier was used, which enabled a higher sensitivity. The pressure in the UHV chamber at position QMS1 during the analog production precludes the use of a more sensitive secondary electron multiplier detector. Specific chemical compounds have been tentatively assigned from mass spectra considering the fragmentation pattern by electron impact ionization available at the NIST database (NIST Mass Spectrometry Data Center et al. 2020).

Morphological characterization of the analogs was performed ex situ by atomic force microscopy (AFM) and transmission electron microscopy (TEM). In both cases the deposits were collected through sample entry 1 of Figure 1. For the AFM measurements the dust analogs were collected on SiO_x substrates whereas carbon grids were employed for TEM. The AFM measurements were carried out with a Cervantes AFM System equipped with Dulcinea electronics from Nanotec Electronica S.L. All images were recorded and analyzed using the WSxM software (Horcas et al. 2007). TEM was performed with a FEI-TITAN X-FEG transmission electron microscope used in scanning mode and operated at 300 kV and at 120 kV. The images were acquired using a high-angle annular dark field detector. The microscope was equipped with a monochromator, Gatan Energy Filter Tridiem 866 ERS, a spherical aberration corrector for the electron probe (which allows for an effective spatial resolution of 0.08 nm), and an energy dispersive X-ray detector for energy dispersive spectroscopy analysis.

The composition of the dust analogs was investigated in situ by infrared spectroscopy in transmission geometry. The dust analogs were deposited on KBr substrates and transferred to a separated UHV chamber by means of a UHV suitcase ($P < 5 \times 10^{-9}$ mbar). This protocol ensured that the inspected deposits were not air-contaminated. A VERTEX 70 V (Bruker)

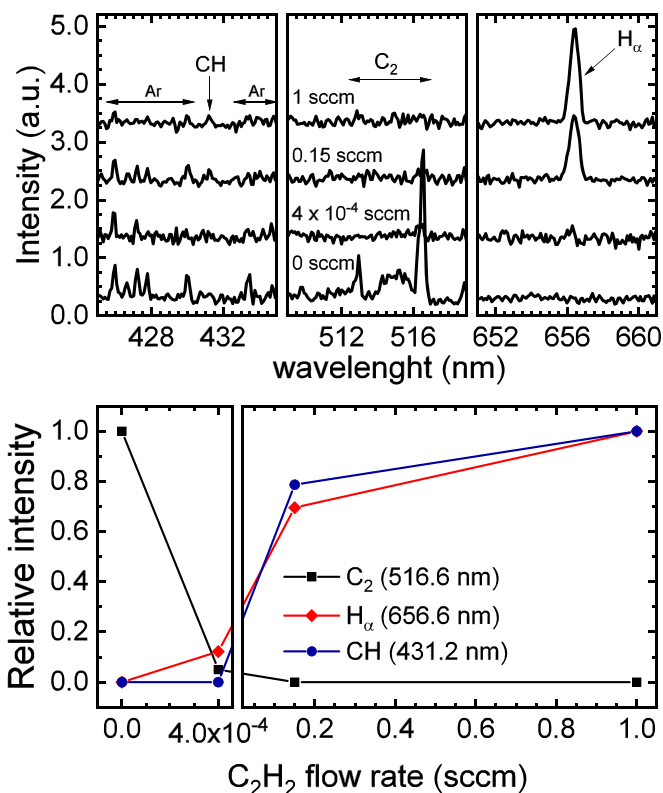


Figure 2. (a) Optical emission spectra in the spectral regions of the CH (A–X) band, C₂ Swan band ($D^3\Pi_g - a^3\Pi_u$), and the H_α line of the Balmer series for the different C₂H₂ flow rates employed. The flow rates are indicated in the figure. The spectra are vertically shifted for clarity. (b) Evolution of the CH, C₂ and H_α line intensities with the C₂H₂ flow rate. The wavelength employed for each line is indicated in the figure.

instrument was employed and the complete optical path was kept in vacuum. The spectral resolution was set to 2 cm^{-1} and 256 scans were coadded. A liquid nitrogen-cooled mercury cadmium telluride detector was used. For the analysis of the IR spectra, spectral deconvolution was performed when peaks were not resolved due to overlapping of IR bands.

Finally, the molecular composition of the analogs was investigated ex situ by laser desorption/ionization mass-spectrometry (LDI-MS) employing the Aromatic Research of Organics with Molecular Analyzer (AROMA) setup (Sabbah et al. 2017) using the so-called laser desorption–laser ionization scheme in which desorption and ionization are separated in time and space and performed with two different lasers. The desorption step was performed with the fundamental mode of a Nd:YAG laser ($\lambda = 1064 \text{ nm}$) whereas the ionization step was performed employing the fourth harmonic of a Nd:YAG laser ($\lambda = 266 \text{ nm}$). This scheme is particularly sensitive to PAHs due to the wavelength of the ionization laser. The ions generated are stored and thermalized in a linear quadrupole ion trap and subsequently monitored by time-of-flight mass spectrometry.

3. Results

3.1. Gas-phase Molecules Produced during Formation of the Dust Analogs

Figure 2(a) shows the optical emission spectra during the dust analog formation inside the aggregation zone of the MICS in the spectral regions corresponding to the CH (A–X) band, the

C_2 Swan band ($d^3\Pi^g - a^3\Pi^u$), and the H_α line of the Balmer series for the different C_2H_2 flow rates employed. When no C_2H_2 was injected inside the aggregation zone, the molecular C_2 Swan band is clearly observed. Since the sputtering of graphite in the SGAS produces mainly atomic carbon, we rationalize that C_2 is formed via the three-body reaction $C + C + Ar \rightarrow C_2 + Ar$ (Martínez et al. 2020), which involves Ar atoms from the sputtering gas used.

As C_2H_2 is injected, the C_2 Swan band vanishes and a clear signature of the presence of atomic hydrogen is observed through the appearance of the H_α line. This suggests that the excited C_2 is consumed to some extent in the reaction $C_2 + C_2H_2 \rightarrow C_4H + H$, which is known to be rapid even at low temperatures (Canosa et al. 2007; Daugey et al. 2008). In addition, as C_2H_2 is injected, it can directly react with atomic carbon through, e.g., $C + C_2H_2 \rightarrow C_3H + H$ and/or $C + C_2H_2 \rightarrow C_3 + H_2$ (Clary et al. 2002), which diminishes the amount of atomic carbon available to form C_2 and releases atomic hydrogen as well. Furthermore, emission from the CH radical is detected for the two highest flow rates investigated. We have already shown that this radical can be formed by the interaction of atomic carbon with H_2 at very low densities, even with the residual H_2 in the UHV chamber (Martínez et al. 2020). The concurrent detection of the H_α line suggests an excess of atomic hydrogen which, if it is not participating in further chemical reactions, will recombine into H_2 by three-body reactions, thus increasing the overall H_2 density. The bimolecular reaction $C + H_2 \rightarrow CH + H$ is highly endothermic unless atomic carbon is electronically excited (Sato et al. 1998). The reaction of C with vibrationally excited H_2 could help in overcoming the barrier energy but under the physical conditions of the Stardust machine we do not expect high abundance of H_2 in the $v = 1, 2$ vibrational levels. Therefore, CH is most probably formed by a three-body reaction involving Ar (sputtering gas) as third body ($C + H + Ar \rightarrow CH + Ar$), although we cannot completely rule out a contribution from the dissociation of C_2H_2 in the magnetron plasma. From gas flow calculations, we have estimated that around 2% of the injected C_2H_2 reaches the magnetron and is therefore susceptible to dissociate by electron impact.

In order to investigate the molecular species that are formed during dust analog production, we have performed in situ mass spectrometry at position QMS1 in Figure 1. Once at this position, no further growth of the analogs takes place. When the production of the analogs is carried out in the absence of C_2H_2 , only Ar, which is used as sputtering gas, and the residual gases in the chamber (H_2 , H_2O and CO) are detected (Figure 3(a)). The peak at $m/z = 80$ corresponds to the formation of Ar dimers (Ar_2) during the gas expansion through the nozzle of the MICS.

In contrast, when C_2H_2 is injected we detect diacetylene (C_4H_2) and for the highest flow rates employed also triacetylene (C_6H_2) (Figure 3(a)). The polymerization of C_2H_2 to larger linear polyacetylenic chains is known to occur through the reaction with the ethynyl radical (C_2H) via $C_2H + C_{2n}H_2 \rightarrow C_{2n+2}H_2 + H$. More interestingly, for the highest C_2H_2 flow rate we have clearly detected C_6H_4 and C_6H_6 (Figure 3(c)). C_6H_4 has been suggested to be involved in the formation of benzene through a cyclization mechanism (De Bleecker et al. 2006a) and the concomitant detection of both species in our experiments seems to support this mechanism.

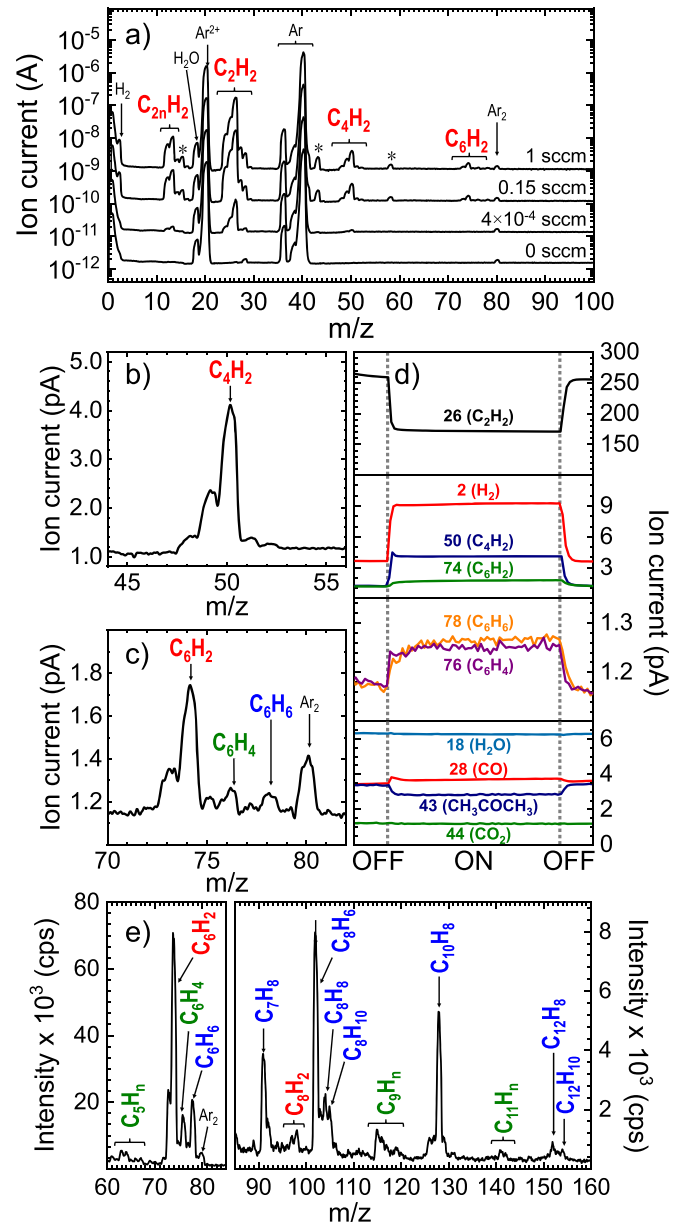


Figure 3. (a) In situ mass spectra at position QMS1 in Figure 1 for the different C_2H_2 flow rates employed (indicated in the figure). The peaks labeled by a star correspond to the acetone impurity of the C_2H_2 gas. The curves have been shifted for clarity. (b, c) Expanded regions for the 1 sccm flow rate. (d) In situ gas-phase detection of $m/z = 2, 18, 26, 28, 43, 44, 50, 74, 76,$ and 78 , which are indicated in the figure along with the assignment to the main contributing chemical species for the 1 sccm flow rate. The dashed vertical lines indicate the switching on and off of the magnetron. (e) In situ mass spectra for the 1 sccm C_2H_2 flow rate at position QMS2 in Figure 1. Peaks labeled in red are assigned to polyacetylenic chains, in blue to aromatic molecules, and in green to aliphatics. In (a) $C_{2n}H_2$ label mass peaks associated to the fragmentation of polyacetylenic chains by electron impact in the quadrupole.

As shown in Figure 3(d), the formation of all the molecules detected by mass spectrometry is accompanied by the consumption of C_2H_2 once atomic carbon is released from the magnetron target. In addition, we have observed the production of H_2 ($m/z = 2$). Atomic hydrogen is produced in high amounts by the polymerization reactions of C_2H_2 , thus it is available to participate in further chemical reactions, including its recombination to molecular hydrogen by three-body reactions.

The signals corresponding to H_2O ($m/z = 18$) and CO_2 ($m/z = 44$) were stable, indicating that they were not involved in the chemical reactions. However, we observed slight changes in the signal associated with the main fragment of acetone ($m/z = 43$), which is present as an impurity in the C_2H_2 (concentration lower than 0.3%), along with a slight increase in the amount of CO ($m/z = 28$). Nevertheless, we did not detect any other gas-phase O-bearing molecule, implying that the acetone impurity in C_2H_2 is only weakly (if any) contributing to the chemistry involved in the formation of the analogs. Moreover, the reaction between C and H_2O has a very large barrier of $\approx 20,000$ K (Mayer et al. 1967) and that of C with CO_2 has been measured at 300 K with a rate below 10^{-15} (Husain & Young 1975); thus, the formation of O-bearing species is very unlikely in our experiments.

Higher-sensitivity gas-phase mass spectrometry was performed at position QMS2 in Figure 1 for the highest C_2H_2 flow rate (Figure 3(e)). The differences observed in the relative intensities among C_6H_2 , C_6H_4 , C_6H_6 , and Ar_2 in Figures 3(c) and (e) are due to the different sensitivity of the QMS as well as the different pressures at locations QMS1 and QMS2. Concerning polyacetylenic chains, we detected up to C_8H_2 . Furthermore, apart from C_6H_6 , we observed the formation of larger aromatic molecules including naphthalene (C_{10}H_8), acenaphthylene (C_{12}H_8), and biphenyl/ethylnaphthalene ($\text{C}_{12}\text{H}_{10}$). These molecules are important for the growth of larger PAHs through different mechanisms including the well-known HACA mechanism (Shukla & Koshi 2012). We have also detected phenylacetylene (C_8H_6) which is a stable intermediate in the growth of naphthalene from benzene through the HACA mechanism. Interestingly, unlike what is observed in acetylene pyrolysis (Shukla & Koshi 2012) or acetylene discharges (Deschenaux et al. 1999), we have detected aromatic molecules with aliphatic substitutions (toluene (C_7H_8), styrene (C_8H_8), and xylene/ethylbenzene (C_8H_{10})). The HACA mechanism does not explain the formation of aromatic compounds with aliphatic substituents. However, the addition of C and its interaction with H_2 (both residual in the UHV system and formed by recombination of the released atomic hydrogen) promotes the formation of alkyl radicals, which open up chemical routes for the formation of alkyl-substituted aromatics (see Section 4).

Finally, we detected a number of hydrogenated carbon clusters (HC-clusters) of aliphatic nature with odd numbers of carbon atoms from C_5 to C_{11} , again differing from what is found in acetylene discharges/pyrolysis in which predominantly molecules with even numbers of carbon atoms are formed (see Figure 3(e)). The apparent absence of C_7 HC-clusters might be due to a blurring of the signal by the peaks associated with toluene and its main fragment ($m/z = 91/92$). For C_3 clusters, it is the Ar signal that precludes its detection. The production of these C-clusters is a clear signature of the interaction of atomic carbon with C_2H_2 . The reaction of C and C_2H_2 is known to be fast, yielding C_3 and/or C_3H (Liao & Herbst 1995; Clary et al. 2002). Analogous reactions of C with larger polyacetylenic chains are also an efficient way to produce hydrocarbons with odd numbers of carbon atoms in chemical environments where C and C_2H_2 are abundant (Cernicharo 2004). In addition, the reaction of C with other large hydrocarbons is known to occur very rapidly and without a barrier (Haider & Husain 1992; Liao & Herbst 1995; Husain & Ioannou 1997).

Table 1

Chemical Species Detected in the Gas Phase by Mass Spectrometry during Production of Dust Analogs along with their Tentative Assignment to Specific Compounds

m/z	Chemical formula	Compound
Polyacetylenic chains		
26	C_2H_2	acetylene
50	C_4H_2	diacetylene
74	C_6H_2	triacetylene
98	C_8H_2	octatetrayne
Aromatics		
78	C_6H_6	benzene
91/92	C_7H_8	toluene
102	C_8H_6	phenylacetylene
104	C_8H_8	styrene
106	C_8H_{10}	xylene/ethylbenzene
128	C_{10}H_8	naphthalene
152	C_{12}H_8	acenaphthylene
153/154	$\text{C}_{12}\text{H}_{10}$	biphenyl/vinylnaphthalene
Aliphatics		
62–68	C_5H_n	C_5 -clusters
76	C_6H_4	3-hexene-1,5-diyne
115–123	C_9H_n	C_9 -clusters
140–144	C_{11}H_n	C_{11} -clusters

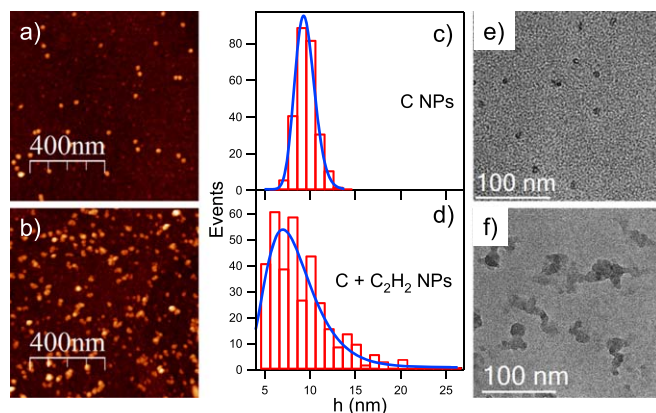


Figure 4. Morphology of the dust analogs without (top) and with (bottom) C_2H_2 injection (flow rate of 1 sccm). (a, b) Atomic force microscopy (AFM) images. (c, d) Size distribution extracted from AFM images. The blue lines correspond to the fitting to log-normal distributions. (e, f) Transmission electron microscopy images.

Overall, the results concerning in situ mass spectrometry evidence the formation of three different families of gas-phase chemical compounds, namely polyacetylenic chains, aromatic species, either pure or with aliphatic substitutions, as well as C- and HC-clusters of aliphatic nature. The identified masses are listed in Table 1 along with their tentative assignments to chemical compounds (NIST Mass Spectrometry Data Center et al. 2020). A detailed description of the possible formation mechanisms is provided in Section 4.

3.2. Morphology of the Dust Analogs

Apart from the gas-phase species, most of the material produced during the formation of the dust analogs consists of particles with diameters in the nanometer range (Figure 4). Due to the low kinetic energy of the particles produced using gas

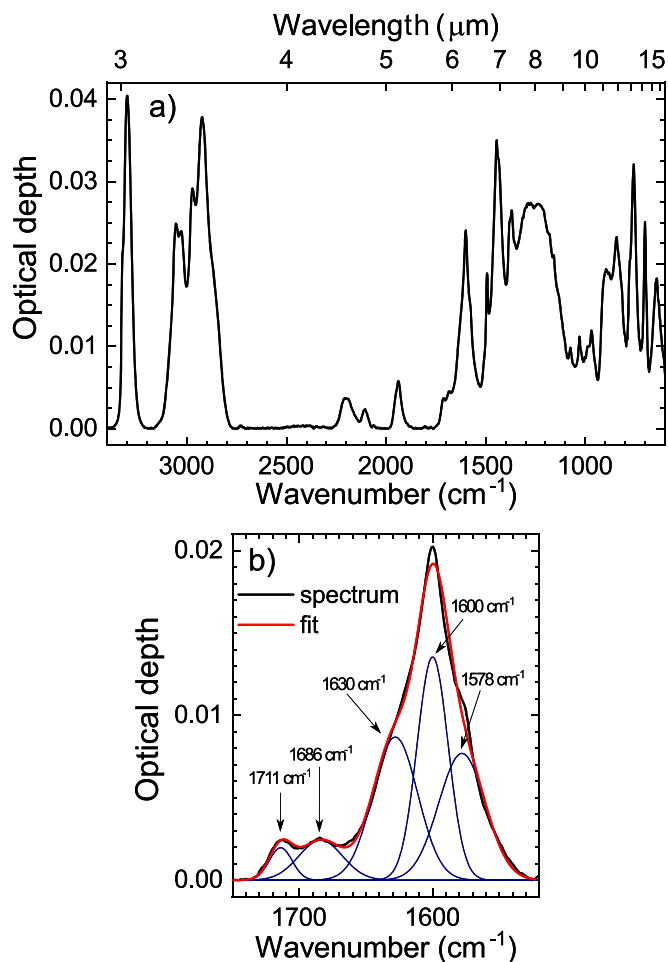


Figure 5. (a) IR spectrum of the dust analog. (b) Spectral deconvolution in the range 1500–1750 cm^{-1} . For the deconvolution, a baseline has been subtracted to remove the contribution from the very broad amorphous carbon band.

aggregation sources, the particles soft-land on the substrate and thus retain the gas-phase morphology and structure.

Figures 4(a) and (b) show typical AFM images of the dust analogs when no C_2H_2 was injected in the aggregation zone (pure C particles) and for a C_2H_2 flow rate of 1 sccm, respectively. In both cases nanoparticles (NPs) are observed with mean NP diameters of 9.3 and 7.0 nm for pure C NPs and for a C_2H_2 flow rate of 1 sccm, respectively. However, a broader size distribution is obtained when injecting C_2H_2 (see Figures 4(c) and (d)). Moreover, the production rate increased enormously when C_2H_2 was injected (by a factor around of 350 in terms of collected NPs/ $\mu\text{m}^2\text{s}$), which evidences the interaction of atomic C with C_2H_2 , resulting in a manifest acceleration of the chemistry.

The TEM analysis of the NPs revealed the formation of amorphous NPs irrespective of the injection of C_2H_2 (Figures 4(e)–(f)). The main difference consists in the shape of the particles. Pure C NPs present a well-defined round shape whereas those formed after C_2H_2 injection tend to agglomerate. This agglomeration is observed in the AFM images as well, but it is more clearly seen in the TEM images. Diffusion of the NPs once deposited on the substrates is not expected, thus the agglomerates might be already formed in the gas phase.

Table 2
Vibrational Band Assignments for the IR Bands with Optical Depth Higher Than 0.0025

ν (cm^{-1})	λ (μm)	Assignment	Intensity
3322	3.01	sp alkyne CH str.	sh
3300	3.03	sp alkyne CH str.	s
3100	3.23	sp^2 arom./olef. CH str.	sh
3085	3.24	sp^2 arom./olef. CH str.	sh
3056	3.27	sp^2 arom./olef. CH str.	m
3029	3.30	sp^2 arom./olef. CH str.	m
2973	3.36	sp^3 asym. CH_3 str.	m-s
2925	3.42	sp^3 asym. CH_2 str.	s
2870	3.48	sp^3 sym. CH_3 str.	sh
2845	3.51	sp^3 sym. CH_2 str.	sh
2200	4.55	sp alkyne CC str. (conjugated alkynes)	w
2105	4.75	sp alkyne CC str	w
1938	5.16	Combination of out-of-plane and in-plane CH bend. modes	w
1800–1000	5.56–10.00	Amorphous carbon (π -band)	m-s
1711	5.84	Carbonyl CO str.	w
1686	5.93	Carbonyl CO str.	w
1630	6.13	sp^2 olef. CC str.	sh
1600	6.25	sp^2 arom. CC str.	m-s
1578	6.34	sp^2 arom. CC str.	sh
1492	6.70	sp^2 arom. CC str.	w
1445	6.92	sp^3 CH_3 asym. bend. / sp^3 CH_2 sci.	m-s
1437	6.96	sp^2 arom. CC str	sh
1379	7.25	sp^3 CH_3 sym. bend.	sh
1369	7.30	sp^3 CH_3 sym. bend.	w-m
1074	9.31	sp^2 arom. CH in-plane bend. / sp^2 olef. CH_2 rock.	w
1029	9.72	sp^2 arom. CH in-plane bend.	w
988	10.12	sp^2 olef. CH wag.	w
968	10.33	sp^3 CH_3 rock.	w
910	10.99	sp^2 olef. CH wag.	sh
890	11.24	sp^2 arom. CH out-of-plane bend. (solo)	m
843	11.86	sp^2 arom. CH out-of-plane bend. (duo)	m
776	12.89	sp^2 arom. CH out-of-plane bend. (trio)	sh
756	13.23	sp^2 arom. CH out-of-plane bend. (quartet)	m-s
700	14.29	sp^2 CH out-of-plane bend.	m
640	15.63	sp^2 arom. CCC in-plane bend.	m

Note. arom: aromatics; olef: olefins. The vibrational modes are abbreviated as str: stretching; bend: bending; sci: scissoring; rock: rocking; wag: wagging. Relative intensities are labeled as s: strong; m: medium; w: weak; sh: shoulder.

3.3. Composition of the Dust Analogs

For the highest C_2H_2 flow rate (1 sccm), we measured the IR spectrum of the dust analogs (Figure 5). The IR spectrum reveals that the sample consists of a complex mixture of hydrocarbons with sp , sp^2 , and sp^3 carbon hybridizations, thus the gas-phase products detected by mass spectrometry are incorporated into the solid dust analogs. The observed infrared bands are listed in Table 2 along with their tentative assignments.

The presence of sp carbon is evidenced by the absorption bands at 3322 and 3300 cm^{-1} corresponding to the $\equiv\text{C}-\text{H}$ stretching modes, and by the band at 2105 cm^{-1} , which

corresponds to the $-C \equiv C-$ stretching mode of monosubstituted acetylene. In addition, a second $-C \equiv C-$ stretching mode is observed at 2200 cm^{-1} which is ascribed to the stretching mode of conjugated triple bonds $-C \equiv C - C \equiv C-$ (Socrates 2001). This band is also found in dust from acetylene plasmas (Stoykov et al. 2001) but is often too weak to be observed (Kovačević et al. 2005; Stefanović et al. 2005). In addition, it is not commonly observed in dust analogs from acetylene pyrolysis (Biennier et al. 2009). The fact that we observe this band might be related to the addition of atomic carbon and the formation of C_2 , which in the end increases the formation of linear polyacetylenic chains via the C_4H radical route (see Section 4).

On the other hand, numerous bands indicate the presence of sp^3 carbon and aliphatic moieties. The bands at 1369 cm^{-1} , 1379 cm^{-1} , and 1445 cm^{-1} , assigned to the CH_3 symmetric bending and CH_3 asymmetric bending/ CH_2 scissoring modes, respectively (see Table 2), are a clear signature of alkyl moieties. These bands are accompanied by those in the region between 3000 and 2800 cm^{-1} , which correspond to the CH_2 and CH_3 stretching modes. Moreover, the band at 968 cm^{-1} is ascribed to the CH_3 rocking mode.

Concerning sp^2 carbon, the bands at 1600 , 1578 , 1492 , and 1437 cm^{-1} reveal the presence of aromatics in the dust analogs. All are assigned to aromatic $C = C$ stretching modes. In the case of alkyl substituted aromatics, the band at 1578 cm^{-1} is usually a shoulder of that at 1600 cm^{-1} , as in our case. Moreover, the band at 1492 cm^{-1} is intense for substituted aromatics (Socrates 2001). These results are consistent with the detection of aromatics with aliphatic substituents by mass spectrometry and reveal that the aromatic compounds incorporated into the dust analogs are not only pure but contain aliphatic substituents as well. We note that a similar result has been recently obtained by Gavilan et al. (2020) during the formation of dust analogs using small PAHs as precursors in a molecular jet exposed to an electrical discharge.

Other bands related to the aromatic compounds incorporated into the dust analogs are the CH out-of-plane bending modes. The different bands observed at 890 cm^{-1} , 843 cm^{-1} , 776 cm^{-1} , and 756 cm^{-1} are related to different numbers of peripheral adjacent H atoms (solo, duo, trio, and quartet, respectively) (Hony et al. 2001; Carpentier et al. 2012) and are characteristic of PAHs, although insensitive to PAH substitution. However, the band at 700 cm^{-1} can be assigned to the CH out-of-plane bending mode of substituted benzenes (Socrates 2001). Finally, the band at 640 cm^{-1} is attributed to the CCC in-plane bending of aromatic compounds (Gadallah et al. 2012) and the combination band at 1938 cm^{-1} is ascribed to the combination of out-of-plane and in-plane CH bending modes (combination and overtone bands in the spectral region 2000 – 1700 cm^{-1} are characteristic of aromatic compounds).

Apart from aromatic compounds, there are also bands related to olefinic sp^2 carbon. The sp^2 CH stretching bands in the region 3100 – 3000 cm^{-1} are due to both aromatic and olefinic sp^2 carbon, but the shoulder at 1630 cm^{-1} is unambiguously assigned to the $C = C$ stretching modes of olefinic compounds (Figure 5(b)) (Socrates 2001; Gavilan et al. 2017). The presence of olefinic moieties is further confirmed by the characteristic wagging modes of olefins at 988 and 910 cm^{-1} (Socrates 2001). The band at 1074 cm^{-1} might be due to the CH_2 rocking mode characteristic of vinyl groups, in accordance with the observation of styrene (and maybe also

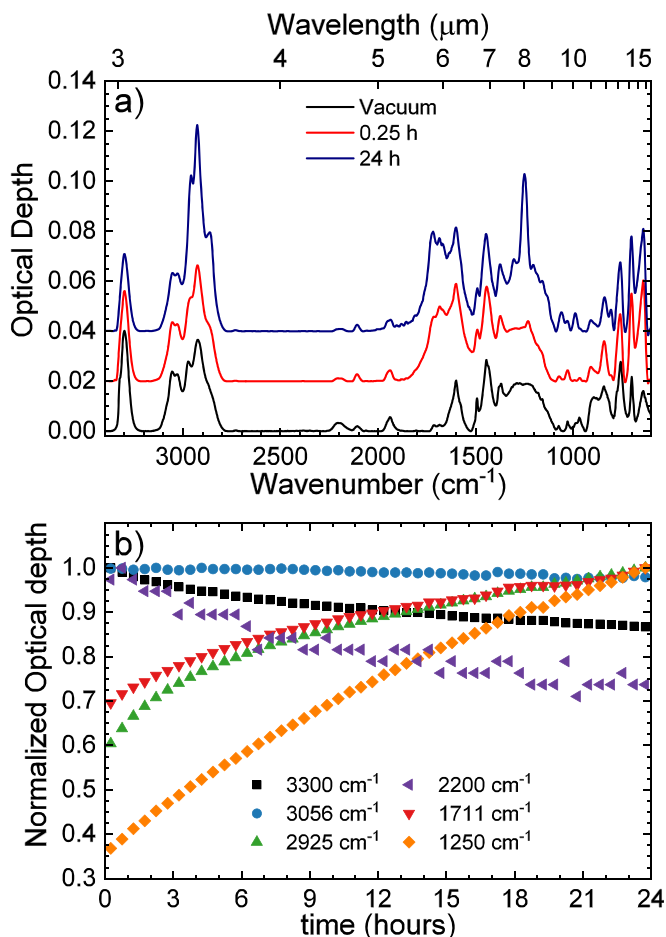


Figure 6. (a) IR spectra of the dust analogs in ultrahigh vacuum and after air exposure for 15 min and 24 hr. The spectra have been vertically shifted for clarity. (b) Temporal evolution of the normalized optical depth for some selected IR bands after exposing the dust analog to air.

vinylanthralene) by mass spectrometry, though the aromatic in-plane CH bending modes overlap in this region.

The broad band that appears in the 1800 – 1000 cm^{-1} region is characteristic of amorphous carbon and its intensity is related to the relative amount of sp^2 to sp^3 carbon hybridization (Ferrari et al. 2003; Rodil 2005). Its presence in the IR spectrum is consistent with the amorphous morphology observed by TEM and suggests that part of the dust analogs are made of amorphous carbon material.

Finally, weak $C = O$ carbonyl stretching bands are observed, which we consider as related to the acetone impurity in the C_2H_2 bottle since the base pressure of the Stardust machine is 10^{-10} mbar and the sample was transferred to the IR UHV chamber by means of a UHV suitcase at a pressure lower than 5×10^{-9} mbar.

In addition, we have tested the stability of the analogs after air exposure and observed that they show a high reactivity (Figure 6), whereas we did not observe any significant change in the IR spectrum of the analogs after 24 hr in UHV. Carbonaceous materials produced from unsaturated precursors are known to react swiftly with oxygen, leading to the formation of $C-O-C$ moieties. Mainly, we have observed the incorporation of oxygen through the increase of the carbonyl $C = O$ stretching modes and through the appearance and growth of a band at 1250 cm^{-1} , assigned to the $C-O-C$ stretching mode. In addition we have observed a reduction in

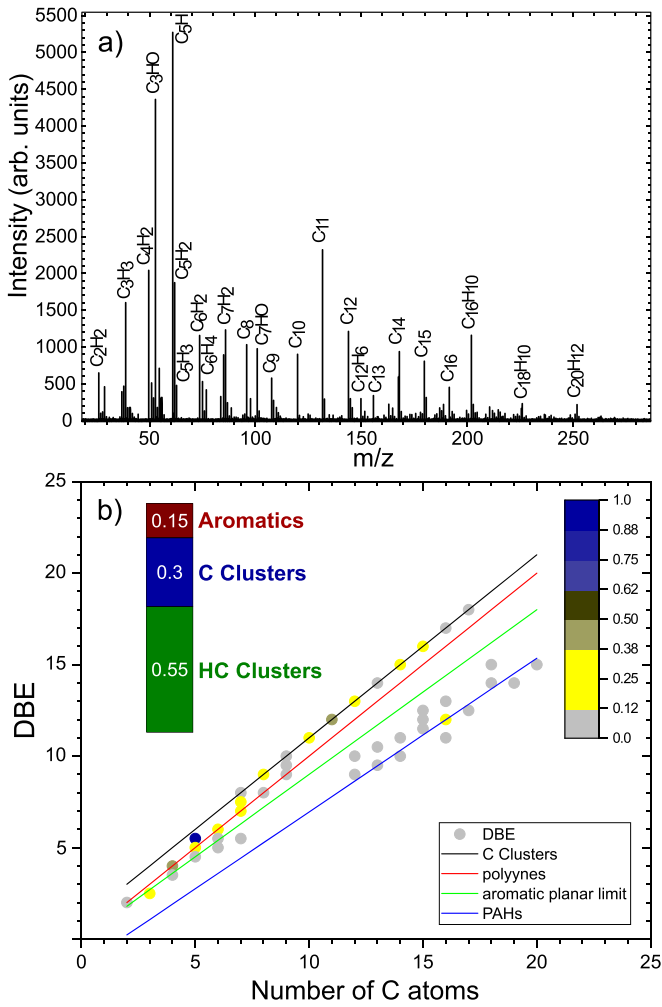


Figure 7. (a) Ex situ LDI-MS of the dust analog using the AROMA setup (Sabbah et al. 2017). (b) Double bond equivalent analysis. The stacked bar graph in the inset summarizes the composition of each molecular family.

the sp carbon content, which is evident from the decrease of the sp CH stretching modes (3300 cm^{-1}) and of the $\text{—C}\equiv\text{C—}$ stretching mode of conjugated alkynes (2200 cm^{-1}). An increase in sp^3 aliphatic moieties was also observed whereas the sp^2 CH stretching modes remain unaltered (see, e.g., the normalized optical depth for the bands at 2925 and at 3056 cm^{-1} in Figure 6(b)). Further changes in the $1000\text{--}600\text{ cm}^{-1}$ region can also be observed, though difficult to interpret. In any case, these results evidence the extreme importance of both working in ultraclean environments (such as UHV conditions) and of in situ characterizing the dust analogs produced from acetylene.

Albeit the tested chemical reactivity of the dust analogs toward atmospheric air, we have performed ex situ LDI-MS of the dust analog produced with a C_2H_2 flow rate of 1 sccm (Figure 7), using the AROMA setup (Sabbah et al. 2017). The results are not quantitative in terms of the relative amount of the observed compounds because of the known chemical evolution of the analogs after air exposure, but they provide additional information on the chemical composition.

Linear polyacetylenic chains (in cationic form) were detected up to C_8H_2 , which is somehow surprising due to the high volatility of these compounds and indicates that these species are trapped inside the dust particles and released by laser

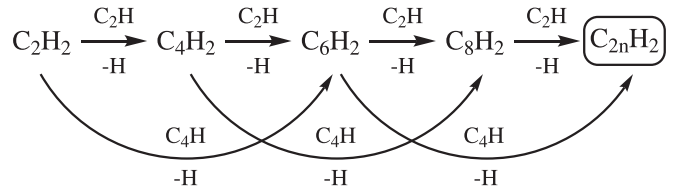


Figure 8. Reaction pathway for the formation of linear polyacetylenic chains.

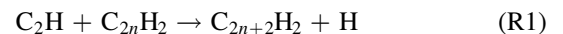
desorption. Other volatile species detected by in situ mass spectrometry, such as benzene or toluene, were not detected by LDI-MS despite the high sensitivity of the technique to aromatics (Sabbah et al. 2017). C_6H_4 could be identified, which was also detected by in situ mass spectrometry and is an important molecule for the formation of benzene. Moreover, C_2H_2^+ and C_3H_3^+ are believed to be produced during the laser desorption stage from the common C_3H_2 precursor (see the supplementary material in Martínez et al. 2020).

On the other hand, C- and HC-clusters with carbon atoms from 5 to 20 dominate the mass spectrum, with C_5H and C_{11} particularly abundant. Relatively large aromatics are also present in the dust analog from C_{12}H_8 (acenaphthylene) to $\text{C}_{20}\text{H}_{12}$. Finally, the peaks assigned to C_3HO and C_7HO evidence oxidation of the sample likely due to air exposure. The results from LDI-MS are summarized in Figure 7(b) by using a double bond equivalent (DBE) analysis. Briefly, in the case of hydrocarbons, DBE can be defined as the sum of the number of double bonds involving carbon plus the number of rings for a particular species. A description of the DBE analysis can be found in, e.g., Sabbah et al. (2017), Gavilan et al. (2020), and in the supplementary information of Martínez et al. (2020). Three molecular families, namely aromatics, HC-, and C-clusters, were considered and their relative intensities in terms of summed peak intensities are shown.

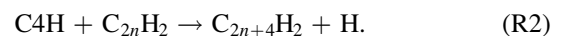
4. Discussion

4.1. Formation of Polyacetylenic Chains (C_{2n}H_2)

Linear polyacetylenic chains, C_{2n}H_2 , are observed in the outer layers around C-rich stars and their formation involves the ethynyl radical (C_2H), which is formed by the photodissociation of C_2H_2 in the outer layers of the CSE and triggers the chemistry of linear polyacetylenic chains (Cernicharo 2004; Agúndez et al. 2017). Once the C_2H radical is formed, the formation of polyacetylenes proceeds mainly through reactions of the type



which are assumed to occur fast at low temperatures (see the scheme in Figure 8) (Chastaing et al. 1998; Agúndez et al. 2017). A second important chemical route for the formation of triacetylene and larger polyacetylenic chains involves the radical C_4H through reactions of the type (Berteloite et al. 2010; Agúndez et al. 2017)



Besides the photodissociation of diacetylene, the C_4H radical can be efficiently formed by the interaction with dicarbon through the bimolecular reaction



In CSEs around C-rich AGB stars, the interaction of C_2H_2 with energetic radiation can lead to dissociation but also to

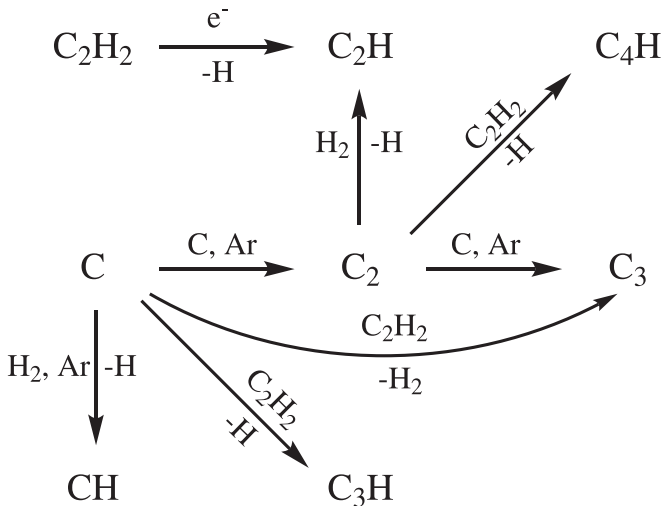


Figure 9. Formation mechanism of radicals from atomic carbon and acetylene in the SGAS. Molecular hydrogen is both residual in the ultrahigh vacuum system and formed by recombination of the released atomic hydrogen.

ionization. Taking into account that ion–neutral reactions are usually faster than neutral–neutral reactions (e.g., the rate constant of $C_2H_2^+ + C_2H_2 \rightarrow C_4H_2^+ + H_2$ is 2.5–5 times higher than that of $C_2H + C_2H_2 \rightarrow C_4H_2 + H$; Anicich 1993; Chastaing et al. 1998), chemical reactions involving ions may also play a role in the synthesis of polyacetylenic chains. The polymerization of C_2H_2 in the external layers is dominated by neutral–neutral reactions involving C_2H , rather than by ion–molecule reactions involving $C_2H_2^+$, because photodissociation of C_2H_2 by the interstellar UV field is 5–10 times faster than photoionization (Heays et al. 2017; Agúndez et al. 2018). However, in the inner clumps of CSEs, where dust acts as an efficient shield against UV photons but cosmic rays can penetrate, some C_2H_2 may be chemically processed due to cosmic-ray-induced ionization and further ion–molecule reactions. The C-star envelope IRC +10216 is known to present a clumpy structure (Cernicharo et al. 2015) and, in fact, cation–neutral reactions have been suggested to play a role for the formation of, e.g., CH_3CN , SiH_3CN , and CH_3SiH_3 (Agúndez et al. 2008; Cernicharo et al. 2017). However, the measured abundances of ions (cations and anions) is very low ($X \leq 10^{-10}$), precluding an important role in the chemistry of the most abundant carbon-bearing species (note that the anions of all C_nH radicals have been detected in the external, cold layers of the envelope but not in the inner, warm regions).

In our experiments, as mentioned in the previous section, we estimate that around 2% of the injected acetylene reaches the magnetron and can therefore be dissociated into C_2H by electron impact (see Figure 9 for a scheme on the formation mechanism of radicals from atomic carbon and acetylene in the SGAS). The interaction of C_2 with H_2 (either residual in the chamber as well as produced by recombination of the atomic hydrogen in excess) contributes also to the formation of the C_2H radical via the bimolecular reaction $C_2 + H_2 \rightarrow C_2H + H$ (Cernicharo 2004; Martínez et al. 2020). In addition, and due to the higher cross section for electron impact ionization over electron impact dissociation (Mao et al. 2008), chemical reactions involving cations such as $C_2H_2^+$ and C_2H^+ might take place. However, the electron temperature of the plasma in magnetron sputtering discharges and in SGASs is lower than 10 eV (Ivanov et al. 1992; Kousal et al. 2017), which favors

electron impact dissociation over direct ionization or dissociative ionization events. This is different to the case of dusty plasmas in which apart from the neutral dissociative production of C_2H , there is a higher probability for the formation of $C_2H_2^+$ (from C_2H_2) and C_2H^+ (from C_2H) by electron knocking-off and dissociative ionization processes, respectively. Thus, the chemistry of the formation of NPs in C_2H_2 dusty plasmas presents a nonnegligible ion–neutral contribution (Jiménez-Redondo et al. 2019). In addition, anionic polymerization routes can be relevant in acetylene plasmas (Deschenaux et al. 1999; De Bleecker et al. 2006b; Jiménez-Redondo et al. 2019) due to the trapping of negative ions in the plasma potential, despite the electron attachment probability being several orders of magnitude lower than those for electron impact dissociation/ionization. However, the chemistry involving anions is very unlikely in SGASs, in which it has been shown that the chemistry proceeds predominantly by neutral–neutral interactions (Haberland et al. 1991; Martínez et al. 2020).

On the other hand, the results from OES suggest that the excited C_2 is consumed to some extent in the reaction (R3) to produce the C_4H radical. Therefore, during the production of the dust analogs the growth of polyacetylenic chains involves mainly the C_2H and C_4H radicals (Figure 8). Moreover, the incorporation of conjugated polyalkynes to the dust analogs in higher amounts than those observed in acetylene discharges, as probed by IR spectroscopy, supports a significant contribution of the C_4H chemical route, which is initiated by the addition of atomic carbon and subsequent formation of C_2 in substantial amounts.

All the abovementioned reactions leading to the growth of polyacetylenic chains release either atomic or molecular hydrogen, which is consistent with the observed increase in the peak at $m/z = 2$ (Figure 3(c)) and with the increase of the H_α line in the optical emission spectra (Figure 2(a)), being therefore available in high amounts to participate in further chemical reactions. We assume that the atomic hydrogen that is not consumed in chemical reactions is recombined into H_2 by three-body reactions involving both Ar and the solid dust analogs.

4.2. Formation of PAHs

Benzene formation is considered as the bottleneck for the growth of PAHs, which have been proposed as the carriers of the AIBs and the seeds of carbonaceous cosmic dust. Benzene has been detected in PPNe (Cernicharo et al. 2001b; Malek et al. 2011) but not yet in the CSE of C-rich AGB stars, which constitute the main factories of cosmic dust. In addition, no specific PAH structure has been identified from observations. In particular, the apolar (or weakly polar) character of these molecules, along with large rotational partition functions, hinder its detection by rotational emission spectroscopy (e.g., Joblin & Mulas 2009). Recently, benzonitrile has been detected in the ISM (McGuire et al. 2018), whose formation might be linked to cyanopolynes in the same manner as benzene is believed to be related to polyynes.

Despite the lack of successful detection of benzene or PAHs in CSEs around C-rich AGB stars, a bottom-up chemical pathway, derived from combustion experiments, has been proposed for the formation of benzene and PAHs in the warm inner regions of C-rich CSEs (Cherchneff et al. 1992; Cherchneff 2012). In this scheme, the key reaction is the direct recombination of two propargyl radicals to form both

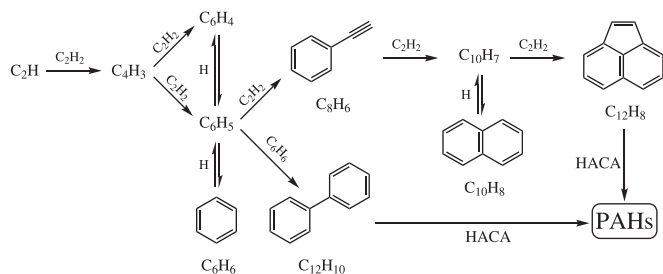
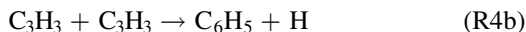
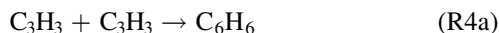


Figure 10. Reaction pathway for the formation of PAHs.

cyclic and linear C_6H_6 as well as the phenyl radical (C_6H_5):



reaction (R4a) being more efficient than (R4b). A different chemical scheme involving hydrocarbon ions has been proposed to explain the formation of benzene in the protoplanetary nebula CRL 618 (Woods et al. 2002), where C_6H_6 has been detected. In this scheme, the synthesis is initiated with proton transfer to C_2H_2 to form $C_2H_3^+$, followed by successive reactions with C_2H_2 to form cyclic $C_6H_5^+$, and ending with the reaction of $C_6H_5^+$ with H_2 to form $C_6H_7^+$, which yield benzene upon dissociative recombination with electrons.

Apart from a top-down etching process (Merino et al. 2014) not considered here, another possible bottom-up mechanism for the formation of benzene involving neutral–neutral reactions has been derived from plasma discharges (De Bleeker et al. 2006a). In this case, C_2H , which is also crucial to the formation of polyacetylenic chains, initiates the chemistry mainly by the termolecular association reaction



where M stands for a third body.

In our case, due to the temperatures involved in the sputtering process in the SGAS (in the order of 500 K) we rule out the formation of benzene via propargyl radicals (note that the $C_3H_3^+$ observed by LDI-MS is formed during the laser desorption step by protonation of C_3H_2). In fact, the concurrent detection of C_6H_4 and C_6H_6 by in situ mass spectrometry points toward a similar neutral–neutral route as that proposed for C_2H_2 discharges, involving C_2H and the formation of the butadienyl radical (C_4H_3). Moreover, the formation of C_4H_3 is less efficient than that of C_4H_2 , which explains the observation of C_6H_6 only at the higher C_2H_2 flow rates employed in our experiments. Once C_4H_3 is formed, the main reactions with C_2H_2 produce C_6H_5 and C_6H_4 (Figure 10), which account for about 75% and 25% of the reaction mechanism toward C_6H_6 , respectively (De Bleeker et al. 2006a). In our case, the detection of C_6H_5 is hindered due to the location of the mass spectrometers, which only allows stable species to be detected.

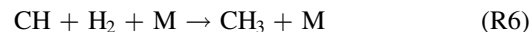
Once C_6H_6 is formed, the growth toward PAHs has been considered in astrophysical models to proceed by the so-called HACA mechanism in which acetylene is the main species propagating the growth of aromatic rings (Figure 10). In addition, the HAVA mechanism (Zhao et al. 2018) and fusion of PAHs (Shukla & Koshi 2010) have been proposed for the growth of large benzoid PAHs. However, none of them explains the formation of aromatics with aliphatic substituents (except those of acetylenic nature), such as those observed in our experiments, both in the gas phase (by in situ mass

spectrometry) and in the solid dust analogs (by in situ IR spectroscopy).

4.3. Formation of Alkyl-substituted Aromatics

Alkyl-substituted aromatics have been proposed to be present in space based on the analysis of the 3.3/3.4 μm band intensity ratio (Joblin et al. 1996). Li & Draine (2012) estimated an upper limit of around 15% for the aliphatic fraction in PAHs derived from the intensities of the 3.4 and 6.85 μm emission features. The formation of alkyl-substituted aromatics is expected to involve the reactivity of the methyl radical (CH_3) with aromatic units and/or aromatic radicals (Shukla et al. 2010).

In CSEs around C-rich AGB stars, CH_4 has been detected (Keady & Ridgway 1993) and it is likely that methyl radicals are present, although they have not been detected and their abundance is unknown. Chemical equilibrium predicts a relatively low abundance of 10^{-9} relative to H_2 in the stellar atmosphere (Agúndez et al. 2020), and unfortunately chemical kinetics models of the inner wind (e.g., Cherchneff 2012) have not provided abundance estimates for CH_3 . A bottom-up synthesis of CH_3 must involve the methylidyne radical (CH), which might arise from the interaction of atomic carbon with molecular hydrogen via $C + H_2 \rightarrow CH + H$. However, this reaction is endothermic by about 100 kJ mol^{-1} and necessitates temperatures in the range of several thousand kelvin to be efficient. Thus, shock-wave-induced chemistry would be needed to efficiently form the methylidyne radical from a bottom-up approach. Once CH radicals are formed, the interaction with H_2 through the reaction



where M stands for a third body, can lead to CH_3 . If this is the case, cosmic dust might be needed as third body to efficiently produce CH_3 . On the other hand, CH_3 radicals can be formed in the outer layers of the CSE by photodissociation of CH_4 in the same way as C_2H radicals are formed from C_2H_2 .

Methylated species have been detected in the C-star AGB IRC+10216 (Cernicharo et al. 2000, 2017; Agúndez et al. 2015). However, their low abundances suggest that they play a minor role in the chemistry of the envelope. A different situation has been found in the CRL618 PPN, where methylpolyynes (CH_3C_2H and CH_3C_4H) have been detected with abundances much larger than those observed in IRC +10216 (Cernicharo et al. 2001a)

Aromatic compounds with aliphatic moieties are neither produced in acetylene pyrolysis (Shukla & Koshi 2012) nor detected (or only very marginally) as neutral species in the gas phase of acetylene discharges (Deschenaux et al. 1999; Consoli et al. 2008). However, this is drastically different when other hydrocarbons are used, particularly in ethylene pyrolysis and ethylene plasmas (Jäger et al. 2006; Gillon & Houssiau 2014). This is related to the formation of alkyl radicals which enter into the chemistry, thus promoting the formation of alkyl moieties. Shukla et al. (2010) demonstrated that pyrolysis of aromatics in the presence of CH_3 radicals can lead to aromatic growth through a methyl-addition cyclization process and Gavilan et al. (2020) have recently proposed a route for PAH growth at low temperatures (150–200 K) by the addition of alkyl radicals.

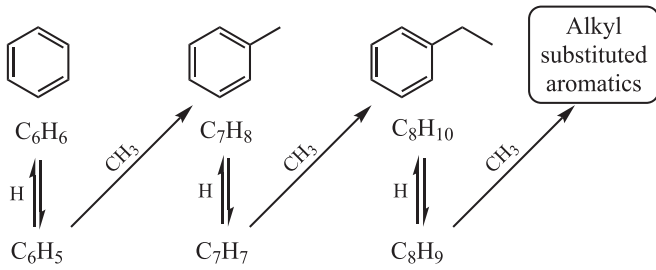
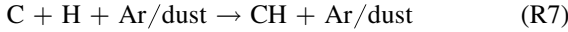


Figure 11. Reaction pathway for the formation of alkyl-substituted aromatics through hydrogen abstraction and subsequent methyl addition.

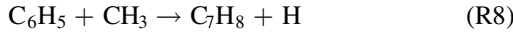
In our case, the CH radical, which we observe by OES, is formed by the reaction



involving Ar and the solid dust analogs as third body.

Once the CH radical is formed, subsequent three-body associations with atomic H would lead to CH_3 . This chemical route continues to the formation of CH_4 , but the acetone impurity in the C_2H_2 bottle prevents its detection by in situ mass spectrometry. Nevertheless, we have recently demonstrated the formation of CH_4 and C_2H_4 by the interaction of atomic C and H_2 even at very low H_2 concentrations (Martínez et al. 2020).

The formation of toluene (C_7H_8) proceeds then by the reaction of phenyl (C_6H_5) and methyl (CH_3) radicals through



the phenyl radical being formed as shown in Figure 10.

The growth toward longer alkyl-chain substitutions to form, e.g., ethylbenzene (C_8H_{10}) proceeds through hydrogen abstraction and methyl addition. This process is not limited to the phenyl radical but applies to any other aromatic radical formed during the growth of PAHs through the HACA mechanism (e.g., naphthyl: C_{10}H_7 , acenaphthyl: C_{12}H_7 , ...) and provides a route for the growth of alkyl-substituted PAHs (Figure 11), closely related to the methyl-addition cyclization mechanism (Shukla et al. 2010).

On the other hand, the likely detection of styrene (C_8H_8) (maybe vinylnaphthalene ($\text{C}_{12}\text{H}_{10}$) as well) by in situ mass spectrometry along with the identification of olefins by IR spectroscopy (including a band likely related to vinyl moieties) points toward the production of the vinyl radical (C_2H_3). Bimolecular reactions involving C, C_2H_2 , and H_2 to form C_2H_3 are highly endothermic for all the possible chemical routes. The same holds for the addition of C_2H_3 to PAHs and aromatic radicals. Therefore, we assume that the formation of aromatics with vinyl substitutions proceeds by three-body reactions involving both Ar and the solid dust analogs.

4.4. Formation of C-clusters with Odd-C Atoms

Molecules and carbon clusters with odd numbers of carbon atoms have been detected in the circumstellar environments of C-rich stars (Hinkle et al. 1988; Bernath et al. 1989) as well as in interstellar clouds (Maier et al. 2001). However, the growth of carbon clusters from C and C_2 at the temperatures found in the CSE is still not well characterized since most chemical reactions involving small C-clusters are still unknown. To date only the $\text{C}_2 + \text{C}_2$ reaction has been measured at high temperature (Kruse & Roth 1997), and has been shown to present a high reaction rate. Therefore, although it potentially

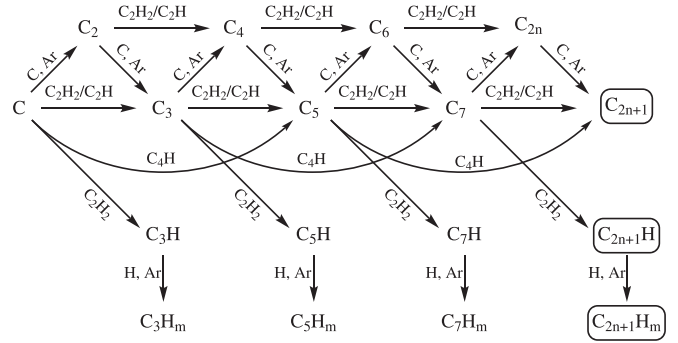
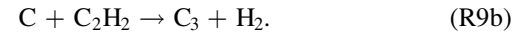
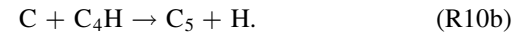


Figure 12. Reaction pathway for the formation of $\text{C}_{2n+1}\text{H}_m$ clusters.

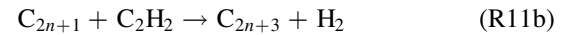
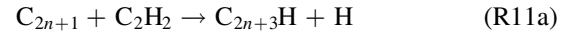
contributes to the chemistry, much is yet to be understood about the role of the $\text{C}_n + \text{C}_m$ reactions in the formation of large C-clusters. An alternative and efficient chemical route is provided by the interaction of atomic carbon with C_2H_2 through the reactions (Cernicharo 2004)



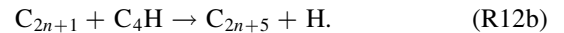
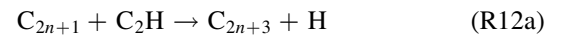
Additionally, C_2H again plays an important role, as in the formation of polyacetylenic chains and benzene, as well as C_4H by the interaction with atomic carbon via



Once C_3 and C_5 are formed by (R9) and (R10), the growth toward larger molecules with odd numbers of carbon atoms proceeds through the following reactions with acetylene:



as well as by the following interactions with C_2H and C_4H :



Therefore, the growth of C-clusters with odd numbers of carbon atoms proceeds through two different chemical routes: an acetylenic route (R11) and a radical route (R12). In fact, these two chemical pathways do not apply only to C_{2n+1} -clusters but also to C_{2n} -clusters, providing a chemical path to the formation of hydrogenated C-clusters.

The abovementioned mechanisms necessitate atomic carbon to initiate the chemistry, which is not present in acetylene combustion experiments or in acetylene discharges. In fact, in particle-forming acetylene discharges the dominant species are by far hydrocarbon molecules with even numbers of carbon atoms (Deschenaux et al. 1999; Kovačević et al. 2003; Consoli et al. 2008; Benedikt 2010). In contrast, the supply of atomic carbon in our case opens up both the acetylenic and the $\text{C}_2\text{H}/\text{C}_4\text{H}$ radical routes described, resembling more closely the mechanism operating in the CSEs of C-rich stars. Figure 12 summarizes the chemical network for the growth of C-clusters. Three-body reactions involving Ar, which cannot be excluded in our experiments, are also shown.



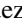



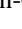
5. Conclusions

In this paper we present a thorough study of the gas-phase chemistry of acetylene in the presence of C and C_2 which can

pertain to the outer layers of C-rich AGB stars and PPNe. We have formed and studied in situ cosmic dust analogs employing atomic carbon and acetylene as precursors, using a well-controlled ultraclean experimental setup. Apart from the formation of linear polyacetylenic chains, we have observed the formation of PAHs. More importantly, aromatics with aliphatic substitutions as well as pure and hydrogenated carbon clusters were produced as a direct consequence of the addition of atomic carbon. The growth of carbon clusters proceeds from the interaction of atomic carbon with acetylene whereas the formation of alkyl-substituted aromatics is rationalized by the formation of methyl radicals and subsequent incorporation into aromatics by a hydrogen abstraction–methyl addition mechanism. In addition, the observed gas-phase species incorporate into the dust analogs, which consist of a complex mixture of sp , sp^2 , and sp^3 hydrocarbons with an amorphous morphology. Our results are of particular interest for unveiling chemical routes leading to formation of acetylene-based molecular species in the external layers of AGB stars and in PPNe, and to foster the search for alkyl-substituted aromatics in these environments.

We thank the European Research Council for funding support under Synergy grant ERC-2013-SyG, G.A. 610256 (NANOCOSMOS). Also, partial support from the Spanish Research Agency (AEI) through grants MAT2017-85089-c2-1R, FIS2016-77578-R, FIS2016-77726-C3-1-P, AYA2016-75066-C2-1-P, and RyC-2014-16277 is acknowledged. Support from the FotoArt-CM Project (P2018/NMT 4367) through the Program of R&D activities between research groups in Technologies 2013, co-financed by European Structural Funds, is also acknowledged. G.T.C. acknowledges funding from the Comunidad Autónoma de Madrid (PEJD-2018-PRE/IND-9029).

ORCID iDs

Gonzalo Santoro  <https://orcid.org/0000-0003-4751-2209>
 Mario Accolla  <https://orcid.org/0000-0002-9509-5967>
 Marcelino Agúndez  <https://orcid.org/0000-0003-3248-3564>
 Hassan Sabbah  <https://orcid.org/0000-0001-5722-4388>
 Christine Joblin  <https://orcid.org/0000-0003-1561-6118>
 José Cernicharo  <https://orcid.org/0000-0002-3518-2524>
 José Ángel Martín-Gago  <https://orcid.org/0000-0003-2663-491X>

References

Agúndez, M., Cernicharo, J., Quintana-Lacaci, G., et al. 2015, *ApJ*, **814**, 143
 Agúndez, M., Cernicharo, J., Quintana-Lacaci, G., et al. 2017, *A&A*, **601**, A4
 Agúndez, M., Fonfría, J. P., Cernicharo, J., Pardo, J. R., & Guélin, M. 2008, *A&A*, **479**, 493
 Agúndez, M., Martínez, J. I., de Andrés, P. L., Cernicharo, J., & Martín-Gago, J. A. 2020, *A&A*, **637**, A59
 Agúndez, M., Roueff, E., le Petit, F., & le Bourlot, J. 2018, *A&A*, **616**, A19
 Allamandola, L., Tielens, A., & Barker, J. 1985, *ApJL*, **290**, L25
 Allamandola, L., Tielens, A., & Barker, J. 1989, *ApJS*, **71**, 733
 Anicich, V. G. 1993, *JPCRD*, **22**, 1469
 Benedikt, J. 2010, *JPhD*, **43**, 043001
 Bernath, P., Hinkle, K., & Keady, J. 1989, *Sci*, **244**, 562
 Bertelote, C., le Picard, S. D., Balucani, N., Canosa, A., & Sims, I. R. 2010, *PCCP*, **12**, 3677
 Biennier, L., Georges, R., Chandrasekaran, V., et al. 2009, *Carbon*, **47**, 3295
 Canosa, A., Páramo, A., Picard, S. D. L., & Sims, I. R. 2007, *Icar*, **187**, 558
 Carpentier, Y., Féraud, G., Dartois, E., et al. 2012, *A&A*, **548**, A40
 Cernicharo, J. 2004, *ApJL*, **608**, L41
 Cernicharo, J., Agúndez, M., Velilla Prieto, L., et al. 2017, *A&A*, **606**, L5

Cernicharo, J., Guélin, M., & Kahane, C. 2000, *A&AS*, **142**, 181
 Cernicharo, J., Heras, A. M., Pardo, J. R., et al. 2001a, *ApJL*, **546**, L127
 Cernicharo, J., Heras, A. M., Tielens, A. G. G. M., et al. 2001b, *ApJL*, **546**, L123
 Cernicharo, J., Marcelino, N., Agúndez, M., & Guélin, M. 2015, *A&A*, **575**, A91
 Chastaing, D. L., James, P. R., Sims, I. W. M., & Smith, I. 1998, *FaDi*, **109**, 165
 Cherchneff, I. 2012, *A&A*, **545**, A12
 Cherchneff, I., Barker, J. R., & Tielens, A. G. G. M. 1992, *ApJ*, **401**, 269
 Cherchneff, I. 2011, in *EAS Pub. Ser. 46, PAHs and the Universe: A Symposium to Celebrate the 25th Anniversary of the PAH Hypothesis*, ed. C. Joblin & A. G. G. M. Tielens (Les Ulis: EDP Sciences), 177
 Chiar, J. E., Tielens, A. G. G. M., Adamson, A. J., & Ricca, A. 2013, *ApJ*, **770**, 78
 Clary, D. C., Buonomo, E., Sims, I. R., et al. 2002, *JPCA*, **106**, 5541
 Consoli, A., Benedikt, J., & von Keudell, A. 2008, *JPCA*, **112**, 11319
 Contreras, C. S., & Salama, F. 2013, *ApJS*, **208**, 6
 Dartois, E., Muñoz Caro, G. M., Deboffle, D., & d'Hendecourt, L. 2004, *A&A*, **423**, L33
 Daugey, N., Caubet, P., Bergeat, A., Costes, M., & Hickson, K. M. 2008, *PCCP*, **10**, 729
 De Bleeker, K., Bogaerts, A., & Goedheer, W. 2006a, *ApPhL*, **88**, 151501
 De Bleeker, K., Bogaerts, A., & Goedheer, W. 2006b, *PhRvE*, **73**, 026405
 Deschenaux, C., Affolter, A., Magni, D., Hollenstein, C., & Fayet, P. 1999, *JPhD*, **32**, 1876
 Ferrarì, A. C., Rodil, S. E., & Robertson, J. 2003, *PhRvB*, **67**, 155306
 Fonfría, J. P., Agúndez, M., Cernicharo, J., Richter, M. J., & Lacy, J. H. 2018, *ApJ*, **852**, 80
 Fonfría, J. P., Cernicharo, J., Richter, M. J., & Lacy, J. H. 2008, *ApJ*, **673**, 445
 Frenklach, M., & Feigelson, E. 1989, *ApJ*, **341**, 372
 Frenklach, M., & Warnatz, J. 1987, *CST*, **51**, 265
 Gadallah, K. A. K., Mutschke, H., & Jäger, C. 2012, *A&A*, **544**, A107
 Gavilan, L., Bejaoui, S., Haggmark, M., et al. 2020, *ApJ*, **889**, 101
 Gavilan, L., Le, K. C., Pino, T., et al. 2017, *A&A*, **607**, A73
 Gehr, R. 1989, in *IAU Symp. 135, Interstellar Dust*, ed. L. J. Allamandola & A. G. G. M. Tielens (Dordrecht: Kluwer), 445
 Gillon, X., & Houssiau, L. 2014, *PSST*, **23**, 045010
 Goto, M., Gaessler, W., Hayano, Y., et al. 2003, *ApJ*, **589**, 419
 Haberland, H., Karrais, M., & Mall, M. 1991, *ZPhyD*, **20**, 413
 Haider, N., & Husain, D. 1992, *Zeitschrift für Physikalische Chemie*, **176**, 133
 Heays, A. N., Bosman, A. D., & van Dishoeck, E. F. 2017, *A&A*, **602**, A105
 Hinkle, K., Keady, J., & Bernath, P. 1988, *Sci*, **241**, 1319
 Hony, S., van Kerckhoven, C., Peeters, E., et al. 2001, *A&A*, **370**, 1030
 Horcas, I., Fernández, R., Gómez-Rodríguez, J. M., et al. 2007, *RSci*, **78**, 013705
 Husain, D., & Ioannou, X. A. 1997, *J. Chem. Soc., Faraday Trans.*, **93**, 3625
 Husain, D., & Young, A. N. 1975, *J. Chem. Soc., Faraday Trans.*, **2**, 525, 71
 Ivanov, I., Statev, S., Orlinov, V., & Shkevov, R. 1992, *Vacuu*, **43**, 837
 Jäger, C., Huisken, F., Mutschke, H., Jansa, I. L., & Henning, T. 2009, *ApJ*, **696**, 706
 Jäger, C., Krasnokutski, S., Staicu, A., et al. 2006, *ApJS*, **166**, 557
 Jiménez-Redondo, M., Tanarro, I., Peláez, R. J., Díaz-Pérez, L., & Herrero, V. J. 2019, *JPCA*, **123**, 8135
 Joblin, C., & Mulas, G. 2009, *EAS Publications Series*, Vol. 35 ed. F. Boulanger et al., 133, doi:10.1051/eas/0935008
 Joblin, C., Tielens, A. G. G. M., Allamandola, L. J., & Geballe, T. R. 1996, *ApJ*, **458**, 610
 Keady, J. J., & Ridgway, S. T. 1993, *ApJ*, **406**, 199
 Kousal, J., Kolpaková, A., Shelemin, A., et al. 2017, *PSST*, **26**, 105003
 Kovačević, E., Stefanović, I., Berndt, J., Pendleton, Y. J., & Winter, J. 2005, *ApJ*, **623**, 242
 Kovačević, E., Stefanović, I., Berndt, J., & Winter, J. 2003, *JAP*, **93**, 2924
 Kruse, T., & Roth, P. 1997, *JPCA*, **101**, 2138
 Kwok, S., & Zhang, Y. 2011, *Natur*, **479**, 80
 Leger, A., & Puget, J. 1984, *A&A*, **137**, L5
 Li, A., & Draine, B. T. 2012, *ApJL*, **760**, L35
 Liao, Q., & Herbst, E. 1995, *ApJ*, **444**, 694
 Maier, J. P., Lakin, N. M., Walker, G. A. H., & Bohlender, D. A. 2001, *ApJ*, **553**, 267
 Malek, S. E., Cami, J., & Bernard-Salas, J. 2011, *ApJ*, **744**, 16
 Mao, M., Benedikt, J., Consoli, A., & Bogaerts, A. 2008, *JPhD*, **41**, 225201
 Martínez, L., Díaz, M., Román, E., et al. 2012, *Langmuir*, **28**, 11241
 Martínez, L., Lauwaet, K., Santoro, G., et al. 2018, *NatSR*, **8**, 7250
 Martínez, L., Santoro, G., Merino, P., et al. 2020, *NatAs*, **4**, 97

- Mayer, S., Schieler, L., & Johnston, H. 1967, *Symposium (International) on Combustion*, 11, 837
- McGuire, B. A., Burkhardt, A. M., Kalenskii, S., et al. 2018, *Sci*, 359, 202
- Merino, P., Švec, M., Martínez, J. I., et al. 2014, *NatCo*, 5, 3054
- Miller, J., & Melius, C. 1992, *CoFl*, 91, 21
- Pascoli, G., & Polleux, A. 2000, *A&A*, 359, 799
- Peeters, E., Hony, S., van Kerckhoven, C., et al. 2002, *A&A*, 390, 1089
- Peeters, E., Spoon, H. W. W., & Tielens, A. G. G. M. 2004, *ApJ*, 613, 986
- Pendleton, Y. J., & Allamandola, L. J. 2002, *ApJS*, 138, 75
- Pilleri, P., Joblin, C., Boulanger, F., & Onaka, T. 2015, *A&A*, 577, A16
- Puget, J., & Leger, A. 1989, *ARA&A*, 27, 161
- Rodil, S. 2005, *DRM*, 14, 1262
- Sabbah, H., Bonnamy, A., Papanastasiou, D., et al. 2017, *ApJ*, 843, 34
- Sato, K., Ishida, N., Kurakata, T., Iwasaki, A., & Tsunashima, S. 1998, *CP*, 237, 195
- Shukla, B., & Koshi, M. 2010, *PCCP*, 12, 2427
- Shukla, B., & Koshi, M. 2012, *CoFl*, 159, 3589
- Shukla, B., Miyoshi, A., & Koshi, M. 2010, *JASMS*, 21, 534
- Socrates, G. 2001, *Infrared Characteristic Group Frequencies* (New York: John Wiley & Sons)
- Stefanović, I., Kovačević, E., Berndt, J., Pendleton, Y., & Winter, J. 2005, *PPCF*, 47, A179
- Stoykov, S., Eggs, C., & Kortshagen, U. 2001, *JPhD*, 34, 2160
- NIST Mass Spectrometry Data Center, William, E., & Wallace, D. 2020, in *NIST Chemistry WebBook*, NIST Standard Reference Database Number 69, ed. P. Linstrom & W. Mallard (Gaithersburg, MD: NIST) doi:10.18434/T4D303
- Woods, P. M., Millar, T. J., Zijlstra, A. A., & Herbst, E. 2002, *ApJL*, 574, L167
- Yang, T., Troy, T. P., Xu, B., et al. 2016, *Angewandte Chemie International Edition*, 55, 14983
- Zhao, L., Kaiser, R. I., Xu, B., et al. 2018, *NatAs*, 2, 413